Regioregular Oligomer and Polymer Containing Thieno[3,4-*b*]thiophene Moiety for Efficient Organic Solar Cells

Yongye Liang,[†] Danqin Feng,[†] Jianchang Guo,[†,‡] Jodi M. Szarko,[§] Claire Ray,[†] Lin X. Chen,*[,‡,§] and Luping Yu*[,†]

Department of Chemistry and The James Franck Institute, The University of Chicago, 929 E. 55th Street, Chicago, Illinois 60637, Chemical Science and Engineering Division, Argonne National Laboratory, Building 200, 9700 S. Cass Ave., Argonne, Illinois 60439, and Department of Chemistry, Northwestern University, Evanston, Illinois 60208

Received October 24, 2008; Revised Manuscript Received December 19, 2008

ABSTRACT: A regioregular conjugated oligomer (MF) and its polymer counterpart (PF) containing a thieno[3,4-*b*]thiophene moiety have been developed. The existence of thieno[3,4-*b*]thiophene extends the absorption of the molecules to longer wavelengths and increases the current density of solar cell devices using these materials. The regioregularity of the polymers from the incorporation of regioregular oligothiophene fragments also enhances hole mobility. Consequently, the polymers show higher solar energy conversion efficiencies in bulk heterojunction (BHJ) solar cells than the low molecular weight oligomers. Spectroscopic and structural studies reveal that composite films prepared from the polymer exhibit a larger charge carrier density and smaller domain sizes for the electron donor and acceptor than the oligomer counterpart. These results rationalize the origin for the higher solar cell efficiency.

Introduction

Bulk heterojunctions (BHJ) are formed in composite materials prepared from a p (or n)-type of organic semiconductor and an electron acceptor (or donor), which are shown to exhibit a significant photovoltaic effect.[1] Solar cells prepared from these materials are attractive for their potential in low cost in manufacturing large-area, lightweight, and flexible devices.[2] However, there are several drawbacks in this type of solar cell which prevent its large-scale commercial applications, such as low solar conversion efficiency and long-term stability.[3] So far, a power conversion efficiency up to 4−5% has been achieved in BHJ solar cells using regioregular poly(3-hexylthiophene) (P3HT) as an electron donor (D) material and [6,6]-phenyl-C61-butyric acid methyl ester (PCBM) as an electron acceptor (A) material.[4] Extensive research has revealed many factors that limit the performance of the BHJ solar cells, such as film morphology and composition, electrode work functions, and surface chemistry of the transparent conductive oxide (i.e., ITO).[5] However, the determining factor in the overall solar cell efficiency is the properties of semiconducting polymers. For example, P3HT only harvests photons with wavelengths below 650 nm, while the energies of the majority of the solar photons are lower and hence are not harvested.[3] Therefore, organic materials with low band gaps are needed for harvesting solar photons in a broader spectrum, particularly in the NIR region. In addition, the low band gap donor material has to possess the following characteristics for achieving high efficiency in device performance: sufficient driving force for exciton dissociation, sufficiently high output voltage, high charge hole mobility, and good miscibility with the electron acceptor (e.g., PCBM) to form an interpenetrating network.[6]

To fulfill these requirements, various design strategies have been pursued. One popular approach is to synthesize copolymers containing alternating monomer units with donor and acceptor characters in the molecule backbone. For example, either benzothiadiazole or thienopyrazine was used as the acceptor unit to form copolymers with an electron-rich thiophene unit. Such low band gap polymers exhibited PV efficiencies of 2−5% in a composite with PCBM.[7] In these systems, a high percentage (over 75% by weight) of a fullerene derivative was usually used. Another useful strategy is to introduce a monomer unit with quinodal character in the conjugated system, which can efficiently reduce the band gap. Fused thiophene ring systems are well-known to stabilize the quinoidal structure.[8] However, several polymers based on such fused-ring systems exhibit poor oxidative stability. Their highest occupied molecular orbital (HOMO) energy level is too high for photovoltaic applications.[9]

Recently, we synthesized an ester-substituted thieno[3,4-*b*]thiophene, which copolymerized with thiophene to form alternating copolymers that showed a rather high external quantum efficiency in the near-IR region.[10] To control the energy levels of the resulting polymers, a series of regiorandom copolymers based on thieno[3,4-*b*]thiophene and thiophene units were synthesized. By varying the ratio of thieno[3,4-b]thiophene to alkyl thiophene units in the copolymers, their electro-optic properties can be fine-tuned. When each of these copolymers was blended with PCBM to form an active layer of a photovoltaic cell, an optimized copolymer composition was found to give the best performance.[11] In order to fully understand the effect of the monomer sequence in the above-mentioned copolymers, we chose to synthesize and study a well-defined oligomer consisted of a well-defined sequence of thieno[3,4-*b*]thiophene and alkylthiophene units and its polymer counterpart with a high molecular weight. Detailed studies on these materials provide valuable knowledge for future development of solar materials of high performances. In particular, we will focus on effects of polymer regioregularity and molecular weight on their optical and electronic properties that are relevant to the device performance.[12]

Results and Discussion

1. Synthesis. The synthetic approach to the oligomer and polymer is shown in Scheme 1. A general approach is to incorporate regioregular oligothiophene on both sides of thieno[3,4-*b*]thiophene to attain regioregular oligomers. Bromination will

* Corresponding authors. E-mail: lchen@anl.gov (L.X.C.); lupingyu@uchicago.edu (L.Y.).
[†] The University of Chicago.
[‡] Argonne National Laboratory.
[§] Northwestern University.

10.1021/ma8023969 CCC: $40.75
Published on Web 01/21/2009

Scheme 1. Synthetic Approach to MF and PF

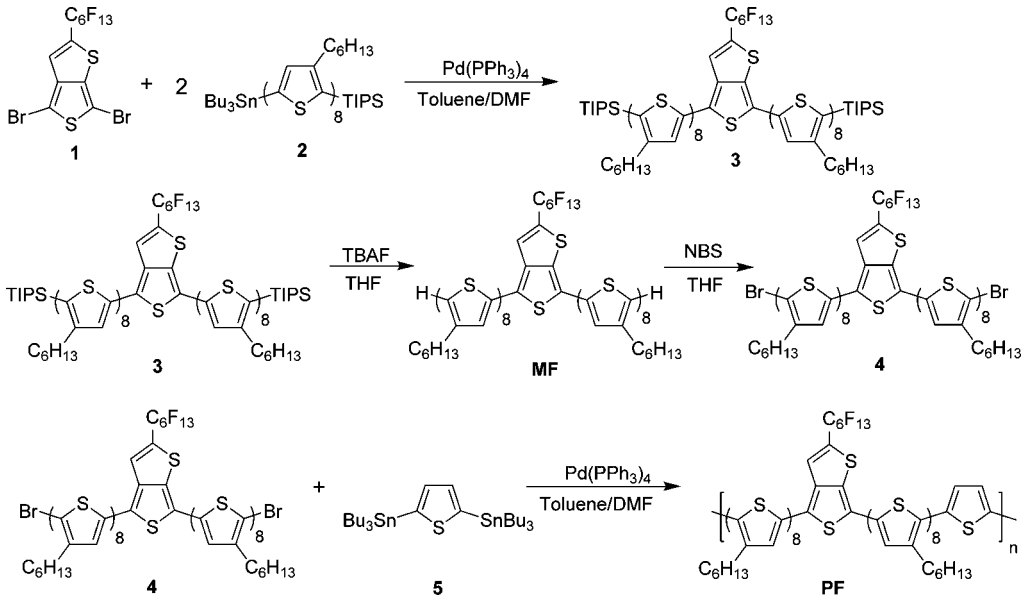

Scheme 2. Synthetic Approach to the Perfluorohexylthieno[3,4-*b*]thiophene Monomer

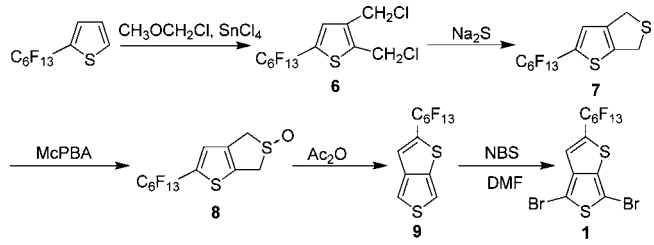

yield the dibromo-substituted oligomer that can be polymerized with ditin-substituted thiophene to produce the regioregular polymers. Initially, we attempted to use ester substituted thieno[3,4-*b*]thiophene to synthesize the polymers. However, our trial on bromination of oligomers failed, as a tribrominated product was obtained with the dibrominated one, and they are not easy to separate. We reason that the thieno[3,4-*b*]thiophene unit is very electron-rich, even with the existence of the ester group. As a result, the proton on the 4-position of the alkylthiophene unit which is next to the thieno[3,4-*b*]thiophene is activated and has similar reactivity as the protons on the 2-position of terminated alkylthiophenes. A new thienothiophene with a more electronegative perfluorohexyl chain was thus synthesized.

The perfluorohexyl-substituted thieno[3,4-*b*]thiophene monomer was synthesized using a similar approach as the ester-substituted monomer reported before[10] (Scheme 2). The Stille coupling reaction between the monomer and 2 equiv of tributyltin-substituted octothiophene followed by deprotection of the triisopropylsilyl (TIPS) group gives the oligomer **MF**. The oligomer can be further converted into dibrominated oligomers by reacting with *n*-bromosuccinimide (NBS). To make sure the oligomer is completely dibrominated, 3 equiv of NBS was used. The mass spectrum only shows the dibrominated product, which indicates that the tribrominated product was not produced in significant quantities. Purification of the oligomers can be easily achieved by simple column chromatography with chloroform as the eluent followed by precipitation in hexanes. Polymerization of the dibrominated oligomer and ditinthiophene via the palladium-catalyzed Stille polycondensation yielded the polymer. The weight-average molecular weight (MW) of the polymer is about 19K, which corresponds to about six repeating units.

The oligomer **MF** is very soluble in chlorinated solvents, such as dichloromethane, chloroform, and chlorobenzene. The polymer **PF** cannot be dissolved in dichloromethane but shows good solubility in warm (over 40 °C) chloroform and chlorobenzene. The **PF** solutions will gel out when cooling down to room temperature for over 1 h. It was found that **MF** can form uniform films by spin-coating from a chloroform solution, but not from a chlorobenzene solution. The polymer (**PF**) can form uniform films by spin-coating from both chloroform and chlorobenzene solutions, but better quality films were obtained from a chlorobenzene solution.

Differential scanning calorimetry (DSC) studies indicated a melting point of 190 °C for **MF** and 238 °C for **PF**. Both **MF** and **PF** are stable up to 400 °C with decomposition temperature (5% weight loss) around 420 °C as was shown by thermogravimetric analysis (TGA) measurements.

2. Optical Properties. The UV−vis absorption spectra of **MF** and **PF** were measured in dilute chlorobenzene solutions as well as in spin-coated films (Figure 1a) with the relevant optical properties summarized in Table 1. Significant red shifts were observed in the lowest energy absorption peaks of **MF** and **PF** films when compared to a regioregular poly(3-hexylthiophene) (rr-P3HT) standard.[13] The band gap calculated from the onset point of the film absorption spectra of **MF** and **PF** is about 0.20 eV smaller than that of P3HT, which demonstrates that the incorporation of the thienothiophene moiety into the oligomer or polymer backbone significantly lowers the material band gap. The enhanced interchain interaction in the films can cause a significant red shift in the absorption

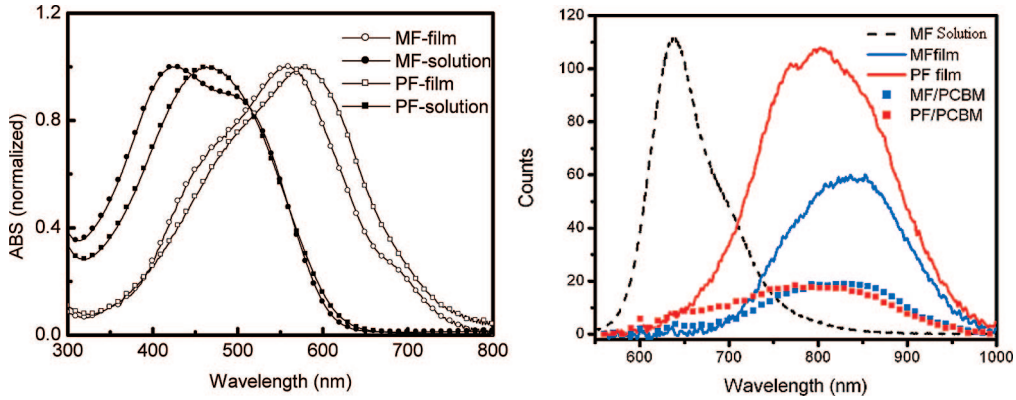

Figure 1. (a) Film and solution absorption spectra of MF and PF (left) and (b) emission spectra of MF, PF, MF/PCBM, and PF/PCBM films (right). The absorption spectra are normalized to better characterize the differences in the peak positions between the materials while emission spectra are normalized with optical densities of the sample to show the quenching effect of PCBM.

Table 1. Optical Properties and Electrochemical Properties of MF and PF

	λ_{max} (nm) sol	λ_{max} (nm) film	λ_{onset} (nm)[a]	E_g (eV)[b]	HOMO (eV)
rr-P3HT[c]	442	504	675	1.84	
MF	426	557	752	1.65	−4.94
PF	463	575	765	1.62	−4.92

[a] Onset point from film absorption spectra. [b] Optical band gap. [c] Regioregular poly(3-hexylthiophene), data from ref 13.

spectra relative to that of the solution samples.[14] Both **MF** and **PF** show >100 nm red shifts from solutions to films, which is much larger than the corresponding shift of 62 nm for P3HT. This red shift indicates that the thienothiophene moiety can enhance the π-conjugation in **MF** and **PF** films due to more rigid backbones that favor interchain packing of the conjugated segments in films. When the **MF** and **PF** films are compared, the latter shows a slightly larger red-shifted absorption as a result of increasing conjugation length.

The emission spectra of **MF** and **PF** samples are shown in Figure 1b. The pristine **MF** film emission spectrum shows one main peak at 835 nm while the emission spectrum of **MF** in a toluene solution shows two main peaks at 640 and 680 nm and a shoulder at 760 nm. The emission spectrum of the pristine **PF** film shows one main peak at 805 nm. The PCBM blended films show a decrease in the emission intensity of the films, which indicates quenching of the emission due to charge transfer. The quenching is more pronounced in the **PF** film than in the **MF** film. When comparing the **MF** and **PF** film spectra, the absorption spectrum of the **PF** film is red-shifted with respect to the **MF** film while the emission spectrum is blue-shifted with a smaller Stokes shift. The red shift in the absorption spectrum is attributed to the increased conjugation length of the polymer with respect to the oligomer. The smaller Stokes shift is most likely due to less steric hindrance for structural reorganization in the excited-state oligomer than in that of the polymer.

3. Electrochemical Properties. The electrochemical properties of **MF** and **PF** were investigated as thin films coated on a glass carbon electrode by using cyclic voltammetry (CV) with a scan rate of 100 mV/s. A Bu_4NPF_6 acetonitrile solution (0.10 M) was used as the electrolyte. Both **MF** and **PF** show a partial reversible oxidation process. The spectra are shown in Figure 2. The onsets of oxidation (φ_{ox}) versus an Ag/Ag^+ electrode for **MF** and **PF** are 0.24 and 0.22 V, respectively. The redox potential of Fc/Fc^+ under the same conditions was used for calibration. The onset of oxidation for this material is located at 0.10 V, which is assumed to have an absolute energy level of −4.80 eV compared to the vacuum level.[15] The HOMO for **MF** was estimated to be −4.94 eV, and **PF** is −4.92 eV. The

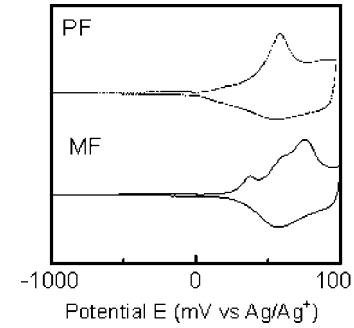

Figure 2. Cyclic voltammetry of PF and MF.

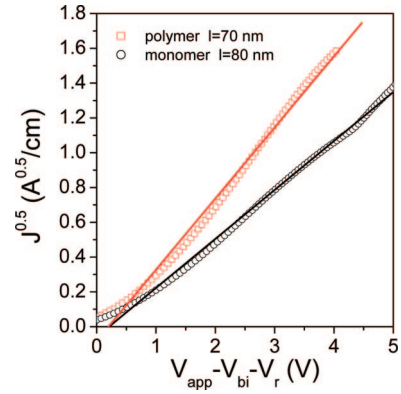

Figure 3. $J^{0.5}$ vs V plots for PF and MF films. The thickness of the films is indicated in the plots. The solid lines are fits of the data points.

HOMO of P3HT measured in the same conditions is −4.90 eV.

4. Hole Mobility. The hole mobility in the polymers is an important factor in determining their performance in organic electronics. An increase in the hole mobility of the polymer increases the average distance the holes travel in the material. As a consequence, thicker films can be fabricated, which increases the light harvesting efficiency in solar cells. We used space charge limited current (SCLC) model to determine the hole mobility in these polymers.[16] The results are plotted in Figure 3 as $J^{0.5}$ vs $(V_{appl} - V_{bi} - V_r)$. The mobility calculated from the SCLC model is 1.9×10^{-4} $cm^2/(V\ s)$ for **PF** and is 1.3×10^{-4} $cm^2/(V\ s)$ for **MF**. The higher mobility of **PF** is most likely due to the extension of electron delocalization lengths in the polymer compared to the oligomer **MF**. More interestingly, the regiorandom polymer with a similar composition ratio of alkyl thiophene to thienothiophene units has a

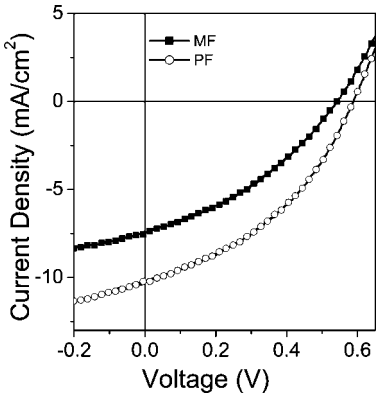

Figure 4. Current−voltage characteristics of polymer solar cells under AM 1.5 conditions (100 mW/ cm^2) from MF/PCBM and MF/PCBM.

Table 2. Photovoltaic Properties of the MF and PF Solar Cells (AM 1.5, 100 mW/cm^2) at Ambient Atmosphere

	J_{sc} (mA/cm^2)	V_{oc} (V)	FF	PCE (%)
PF	10.22	0.59	0.40	2.38
MF	7.42	0.54	0.36	1.46

mobility of 4.8×10^{-5} cm^2/(V s),[11] which shows that the more regioregular structure facilitates charge transport. However, due to the distortion of the conjugated backbone by the steric hindrance from the two H-linked alkyl thiophene rings connected to the thiophene ring, the **PF** mobility is not as high as P3HT with high molecular weight (M_w = 31.1K, mobility of 3.30×10^{-4} cm^2/(V s)).[16]

5. Photovoltaic Properties. The solar cells containing **MF** or **PF** were fabricated with the structure of ITO/PEDOT-PSS/polymer:PCBM/Al, and the PV performance measurements were carried out under an ambient atmosphere. Figure 4 shows the $I-V$ curves of the polymer solar cells under the condition of AM 1.5 at 100 mW/cm^2. Representative characteristics of the solar cells are listed in Table 2. The current density of the **PF**/PCBM solar cell reaches 10.2 mA/cm^2, which is comparable to the reported P3HT/PCBM devices.[5] However, a slightly lower open-circuit voltage and a low fill factor limits its efficiency to 2.4%. The solar cells prepared from **MF** are inferior in their physical performance to the **PF** devices, with a current density of ∼70% of the **PF** solar cells.

In these organic solar cells, heterojunction structures are formed in a blend of oligomers/polymers and fullerene derivatives. Optimization of these heterojunctions requires an interpenetrating bicontinuous network for efficient charge separation, transport, and extraction from the device before charge recombination can occur.[17] The topography of the blended films studied by atomic force microscopy (AFM) studies revealed that the morphology of the **PF**/PCBM blend films exhibited finer features than **MF**/PCBM blend films (Figure 5). In these topography images, nanofibers with diameter ranging from 15 to 20 nm can be found in **PF**/PCBM blend films, while 30−40 nm can be found in **MF**/PCBM. It shows that **PF** has better miscibility with PCBM than **MF**. Because the smaller oligomer molecule can pack better in films, phase segregation between the oligomer and PCBM is more favorable than in **PF**/PCBM. The increased domain sizes account for the inferior performance of solar cells made from **MF** to that from **PF**, which is confirmed in the X-ray diffraction and spectroscopic studies.

6. Molecular Packing Structures in Films Studied by Grazing Incident X-ray Scattering (GIXS). Figure 6 shows the grazing incident small-angle X-ray scattering (GISAXS) and grazing incident wider angle X-ray scattering (GIWAXS) images of the **MF** film in two wavevector regions. The scattering profiles for $q = 0.006-0.155$ Å^{-1} are shown in Figure 6a while Figure 6b shows the scattering profile for $q = 0.14-1.00$ Å^{-1}. The domain spacing was obtained by the relationship $d = 2\pi/q$. In Figure 6a, the broad ring corresponds to an average d-spacing of 6.45 nm. The domain does not show substantial angular dependence in the scattering pattern, which indicates random **MF** orientations in the film with respect to the substrate. The d-spacing of 6.45 nm is comparable to the thiophene chain length in the **MF** molecule. Although this d-spacing is present in all four samples (**MF**, **MF**/PCBM, **PF**, and **PF**/PCBM), it is the most prominent in the **MF** sample. The horizontal line profiles of images of the four thin film samples are shown in Figure 6c. These plots are presented in the log scale to show the presence of a Guinier region in the films containing PCBM. For the **MF**/PCBM film, the Guinier region represents a larger domain than in the **PF**/PCBM sample. A peak is also observed at q ∼0.015, which indicates that these domains are more ordered and closer together in the **MF**/PCBM film. These experiments indicate that there exist larger and more ordered structures in the **MF**/PCBM film than in the **PF**/PCBM film, which will lower the exciton splitting efficiency due to the exciton diffusion length limit in films and can explain the inferiority of the solar cell performance of the **MF**/PCBM composite.

The regularly spaced rings in the wider-angle X-ray scattering pattern of the **MF** film in Figure 6b indicate a d-spacing of 1.65 nm. The larger rings show the higher order diffractions of this domain. The multiple ring scattering patterns indicate a relatively long-range order in the material with the same dimension. The enhanced scattering intensity in the vertical position shows that the domain has a slight tendency to order parallel to the substrate. A similar peak is observed in all four structures (Figure 6b,d). This peak corresponds well to the width of the molecule. When PCBM is added to the samples, the domain is still present, but the signal is lower due to the disorder induced by mixing the two compositions.

7. Charge Separation and Charge Recombination Dynamics of MF/PCBM and PF/PCBM Films. The ultrafast transient absorption spectroscopy probes the dynamics of fundamental processes in PV materials, such as exciton generation, charge separation (CS), charge recombination (CR), etc. These rate constants give insightful understanding on how exciton decay cascade can be effectively used for charge carrier generation in order to optimize solar cell efficiencies from molecular and assembly levels. The CS and CR dynamics of **MF**/PCBM and **PF**/PCBM were measured by ultrafast optical transient absorption (TA) spectroscopy with an excitation wavelength of 600 nm. Figure 7 shows the TA spectra of **PF** and **PF**/PCBM (1:1 weight ratio) films in two spectral regions: 500−740 and 900−1600 nm. A negative ground-state bleaching feature at 594 nm and a broad NIR peak centered at 1230 nm can be observed in **PF** films. The 1230 nm peak can be assigned to the singlet exciton absorption.[19] The ground-state bleaching and exciton absorption features of **MF** are at 577 and 1200 nm (not shown), respectively. The ground-state bleaching peak of **PF**/PCBM composite film shifts to 584 nm within 0.4 ps after the excitation, while the exciton absorption feature shifts to 1210 nm with a shoulder feature appearing at 1060 nm. This feature becomes dominant at longer times while the feature at 1210 nm decays. In the visible region, a broad absorption band above 670 nm rises as early as 0.4 ps, which correlates well with the shift of the **PF** ground-state absorption peak. This broad absorption band is very long-lived and virtually unchanged within a few nanoseconds after excitation. In contrast, the TA spectra of the **PF** polymer film in the absence of PCBM show little absorption in this spectral region. Therefore, the broad

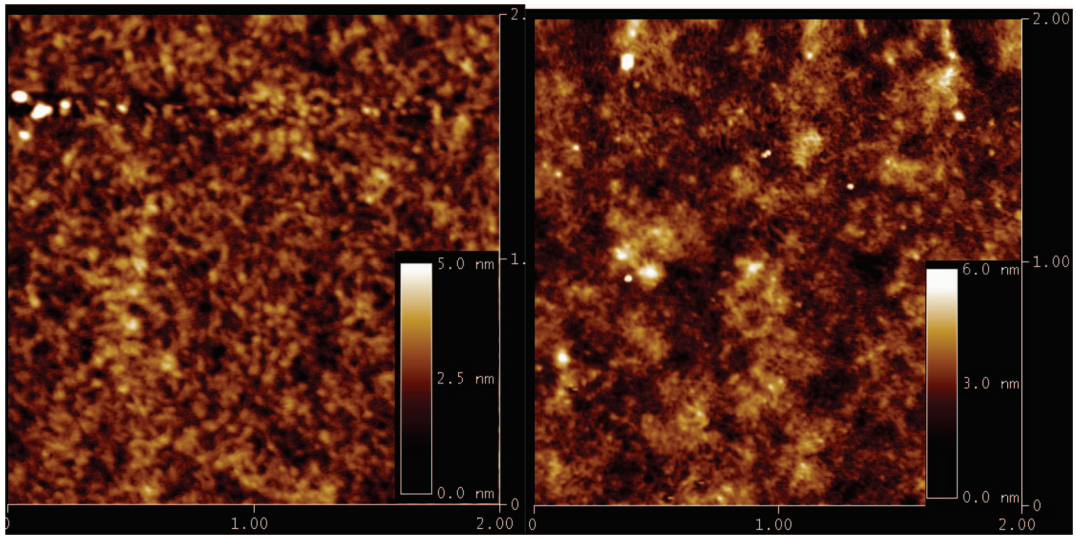

Figure 5. AFM topography images of MF/PCBM (left) and PF/PCBM blend films (2 μm × 2 μm).

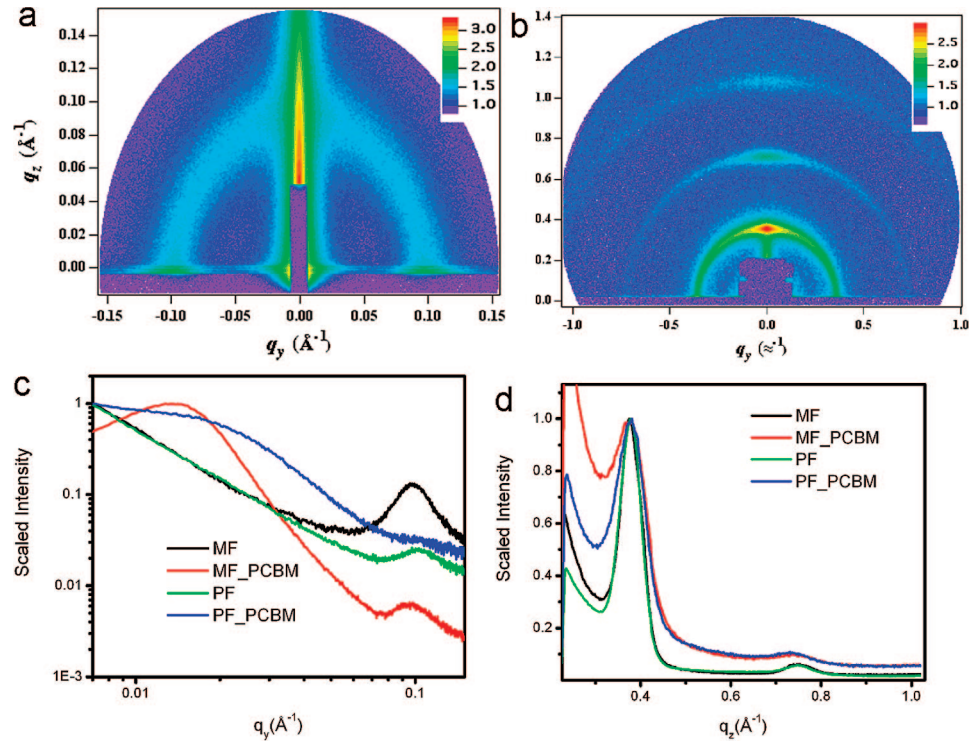

Figure 6. (a) GISAXS and (b) GIWAXS images of the MF thin film. The GISAXS shows a randomly distributed domain 6.45 nm in size while the GIWAXS shows one main peak roughly 1.65 nm in size that is more oriented parallel to the surface of the substrate. (c) Horizontal GISAXS line cut of all four films studied. The films with PCBM show a polydisperse domain 30−40 nm in size, and it is most likely due to PCBM islands in the polymer films. (d) Vertical line cuts of the four films. The vertical line cut was taken to optimize the signal intensity of the plots.

absorption above 670 nm in the visible region and the 1060 nm peak in the NIR region found in the TA spectra of the **PF**/PCBM composite film provide evidence for new species in addition to the singlet exciton observed in the neat **PF** film. On the basis of the in situ electrospectrochemical results (not shown here), we assign the broad peak from 650 to 1060 nm to the cation absorption of **PF** after charge transfer from **PF** to PCBM. The transient spectra of **MF**/PCBM show the cation absorption of **MF** extends from 620 to 1040 nm.

Because the absorption of **MF** or **PF** cation in the NIR region overlaps with the singlet exciton absorption, especially at early delay times, the CS and CR dynamics in **MF**/PCBM or **PF**/PCBM films are monitored by the kinetic traces at 700 nm, where little absorption is observed for neat **MF** and **PF** films. Figure 8 shows the kinetic traces of **MF**/PCBM and **PF**/PCBM films monitored at 700 nm. The traces were normalized by the number of photons absorbed by the films and are fit by a multiexponential function. The **MF**/PCBM film has <120 fs (56%) and 250 fs (44%) charge separation time, and charge recombination is negligible at our 3 ns time window. **PF**/PCBM exhibits a <120 fs (77%) and a 13.4 ps (23%) CS component with CR time at 406 ps (13%) and >3 ns (87%), which indicates that **MF**/PCBM has a faster CS rate and slower CR rate than **PF**/PCBM. However, the cation yield of **PF**/PCBM at 3 ns is about 70% higher than that of **MF**/PCBM. This suggests that the free charge carrier generated in **PF**/PCBM is much higher than **MF**/PCBM. As a result, the **PF**/PCBM cell shows a higher efficiency than the **MF**/PCBM cell although the CS and CR

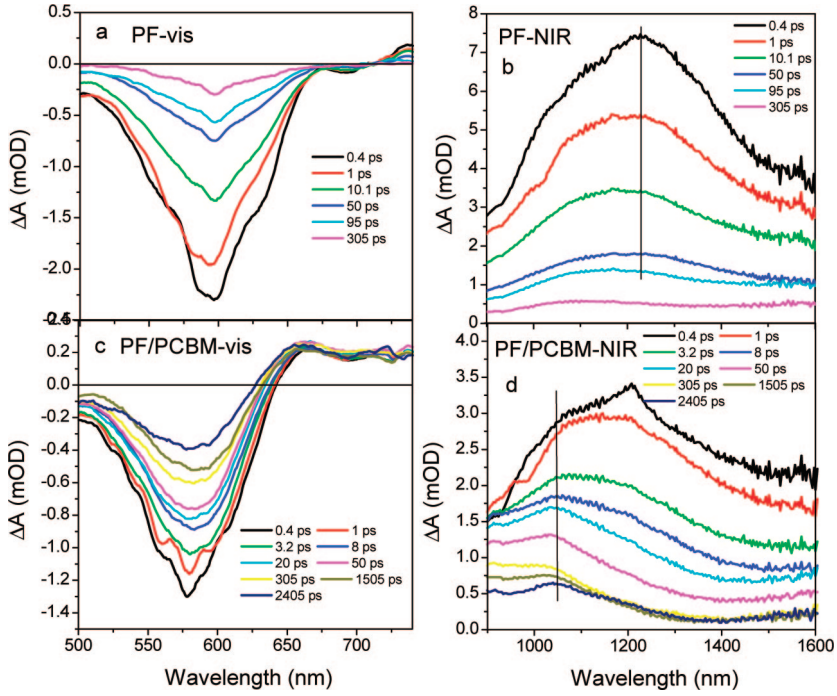

Figure 7. TA spectra of PF at (a) visible probe region and (b) NIR probe region and PF/PCBM at (c) visible probe region and (d) NIR probe region.

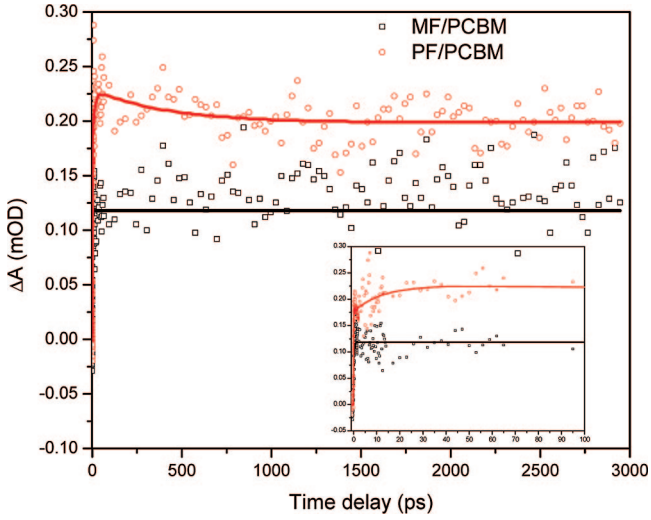

Figure 8. Comparison of CS and CR dynamics of MF/PCBM and PF/PCBM monitored at 700 nm after 600 nm excitation. The traces are normalized by optical absorption at 600 nm to the same amount of photon absorption.

dynamics is more favorable for the **MF**/PCBM cell. The possible low charge carrier yield in the **MF**/PCBM film can be correlated with the lower exciton splitting efficiency due to the larger crystalline domains with sizes exceeding the exciton diffusion length in the film as suggested in the AFM and GIXS results.

Conclusions

A regioregular conjugated oligomer and its corresponding polymer containing a thieno[3,4-*b*]thiophene moiety have been synthesized. The existence of thieno[3,4-*b*]thiophene broadens the absorption spectrum of the molecules to longer wavelengths and increases the current density of their respective solar cell devices. The regioregularity due to incorporation of regioregular oligothiophene enhanced the hole mobility of these materials. Compared to the lower molecular weight oligomers, the polymers showed higher solar conversion efficiency in BHJ type of solar cells. Spectroscopic studies revealed that composite film prepared from **PF** exhibit a larger charge carrier density compared to the oligomer films, which is the origin for the higher solar efficiency.

Experimental Section

General. Unless otherwise specified, all chemicals and reagents were purchased from commercial suppliers and used without further purification. Toluene was distilled over sodium prior to use. 2,5-Bis(tributylstannyl)thiophene was synthesized according to the procedure reported in the literature.[20] Tributylstannyloctothiophene (**2**) was synthesized by a similar procedure reported in the literature.[21] The regioregular poly(3-hexylthiophene) (P3HT) was synthesized and purified according to the method reported by McCullough and co-workers;[22] the obtained P3HT has M_n = 90K and PDI = 1.31, with regioregularity >95%. PCBM was synthesized using the method reported by Wudl and co-workers.[23] ^{1}H NMR spectra were recorded at 400 or 500 MHz (^{13}C spectra at 100 or 125 MHz) on Bruker DRX-400 or DRX-500 spectrometers, respectively. Molecular weights and distributions of polymers were determined by using gel permeation chromatography (GPC) with a Waters Associates liquid chromatograph equipped with a Waters 510 HPLC pump, a Waters 410 differential refractometer, and a Waters 486 tunable absorbance detector. THF was used as the eluent and polystyrene as the standard. The optical absorption spectra were taken by a Hewlett-Packard 8453 UV−vis spectrometer. The emission spectra were measure with an Ocean Optics SD2000 spectrometer. Thin films of the polymers were spin-coated from their solutions in chlorobenzene, and the film absorption spectra were measured. The electrochemical properties of the polymers were investigated by using cyclic voltammetry (CV). The polymer thin films coated on glass carbon electrode were studied in a 0.10 M Bu_4NPF_6 acetonitrile solution with scan rate at 100 mV/s. The Ag/Ag^+ electrode was used as reference electrode.

Synthesis. *2,3-Bis(chloromethyl)-5-perfluorohexylthiophene (**6**).* To a mixture of 4.0 g (10 mmol) of 2-perfluorohexylthiophene and 4.0 g (50 mmol) of chloromethyl methyl ether was added dropwise 4.6 g (18 mmol) of $SnCl_4$ in an ice−water bath, and the mixture was stirred for 5 h at RT after the addition. 50 mL of CH_2Cl_2 was added, and the reaction mixture was poured to

ice−water. The organic phase was washed with brine, dried, and evaporated in vacuo. Column chromatography on silica gel using hexanes yielded the title compound as light yellow oil (4.4 g, 88%). ^{1}H NMR ($CDCl_3$): δ4.61 (2H, s), 4.80 (2H, s), 7.38 (1H, s). MS (EI): Calcd, 497.9; found $(M + 1)^+$, 498.5.

*2-Perfluorohexyl-4,6-dihydrothieno[3,4-b]thiophene (***7***).* A solution of 5.0 g (10 mmol) of **11** in 100 mL of methanol was heated up and kept under mild boiling. Sodium sulfide solution (2.7 g, 11 mmol) in 80 mL of methanol was added dropwise in 1 h. After cooling of the reaction mixture, the precipitate was filtered off. The solvent was removed by evaporation, and the residue was washed by water. Column chromatography on silica gel using hexanes/dichloromethance (3/1) yielded the pure title compound as light yellow liquid (2.5 g, 53%). ^{1}H NMR ($CDCl_3$): δ 4.07−4.09 (2H, t, J = 3 Hz), 4.21−4.23 (2H, m), 7.13 (1H, s). MS (EI): Calcd, 456.0; found $(M + 1)^+$, 456.9.

*2-Perfluorohexylthieno[3,4-b]thiophene (***9***).* A solution of 2.3 g (5.0 mmol) of **12** in 40 mL of ethyl acetate was cooled in a dry ice bath, and then 1.1 g (5.0 mmol) of 3-chloroperbenzoic acid in 20 mL of ethyl acetate was added dropwise. After the addition, the mixture was kept stirring in dry ice bath for 2 h and then RT for 6 h. Removal of solvent under vacuum produced a white solid. The residue contained a crude product of **8** and 3-chlorobenzoic acid. The obtained solid was refluxed in 20 mL of acetic anhydride for 2 h. Then the mixture was cooled down, and solvent was removed under vacuum. Column chromatography on silica gel using hexanes as eluent yielded the title compound as colorless liquid (1.8 g, 80%). ^{1}H NMR ($CDCl_3$): δ 7.33−7.36 (2H, m), 7.57−7.59 (1H, d J = 2 Hz). MS (EI): Calcd, 458.3; found $(M + 1)^+$, 458.9.

*4,6-Dibromo-2-perfluorohexylthieno[3,4-b]thiophene (***1***).* To a solution of 2.75 g (6.0 mmol) of **5** in 15 mL of DMF was added dropwise a solution of NBS (2.70 g, 15.0 mmol) in 15 mL of DMF under nitrogen protection in the dark. The reaction mixture was heated up to 40 °C and kept stirring for 24 h. Then it was cooled down, poured to saturated sodium sulfite solution at ice−water bath, and extracted with dichloromethane. The organic phase was collected and dried by sodium sulfate. Removal of the solvent and column purification on silica gel using hexane as eluent yielded the target product **14** (3.32 g, 90%). ^{1}H NMR ($CDCl_3$): δ 7.20 (1H, s) MS (EI): Calcd, 616.1; found $(M + 1)^+$, 616.7.

MF. The synthetic routes of oligomers and polymer are shown in Scheme 1. Monomer **1** (331 mg, 0.50 mmol) was weighed in a 25 mL round-bottom flask, to which tributylstannyloctothiophene **2** (2.13 g, 1.20 mmol) and $Pd(PPh_3)_4$ (25 mg) were added. The flask was subjected to three successive cycles of evacuation followed by refilling with argon. Then, anhydrous DMF (4 mL) and anhydrous toluene (16 mL) were added via syringe. The reaction was carried out at 120 °C for 24 h. The raw product was collected by precipitating in methanol, and the precipitate was dissolved in THF (20 mL) and cooled in a dry ice bath. TBAF solution (1.8 mL, 1 M) was added dropwise and kept stirring in dry ice bath for 1 h and then at RT overnight. The raw product **17** was collected by precipitating in hexanes. The product was further purified by column chromatography on silica gel using hexanes/methylene chloride as eluent yielded the title compound (1.09 g, 70%). ^{1}H NMR ($CDCl_3$): δ 0.86−0.91 (48H, m), 1.26−1.44 (96H, m), 1.63−1.71 (32H, m), 2.55−2.65 (4H, t, J = 8 Hz), 2.73−2.82 (28H, m), 6.90 (1H, s), 6.96−7.00 (11H, m), 7.02−7.03 (2H, d, J = 4 Hz), 7.07 (1H, s), 7.11 (1H, s), 7.61 (1H, s). MS (MALDI): calcd, 3115.2; found, 3115.6.

Oligomer **4**. A solution of **MF** (0.93 g, 0.30 mmol) in THF (30 mL) was added dropwise to a solution of NBS (0.133 g, 0.75 mmol) in THF (5 mL) under nitrogen protection in the dark. The reaction mixture was constantly stirred for 24 h. The raw product **18** was collected by precipitating in hexanes. The product was further purified by column chromatography on a silica gel using hexanes/methylene chloride as eluent and yielded the title compound (0.83 g, 85%). ^{1}H NMR ($CDCl_3$): δ 0.90−0.91 (48H, m), 1.25−1.54 (96H, m), 1.63−1.72 (32H, m), 2.55−2.59 (4H, t, J = 8 Hz), 2.73−2.80 (28H, m), 6.69 (2H, s), 6.82−7.11 (12H, m), 7.61 (1H, s). MS (MALDI): calcd, 3271.1; found, 3272.8.

PF. Oligomer **4** (327 mg, 0.10 mmol) was weighed in a 25 mL round-bottom flask, to which 2,5-bis(tributylstannyl)thiophene (66 mg, 0.10 mmol) and $Pd(PPh_3)_4$ (5 mg) were added. The flask was subjected to three successive cycles of evacuation followed by refilling with argon. Then, anhydrous DMF (2 mL) and anhydrous toluene (8 mL) were added via syringe. The polymerization was carried out at 120 °C for 24 h. The raw product was collected by precipitating in methanol, and the precipitate was dissolved in chloroform and filtered with Celite to remove the metal catalyst. The final polymers were obtained by precipitating in hexanes and drying in vacuum for 12 h, yielding solid (288 mg, 90%). ^{1}H NMR ($CDCl_3$): δ 0.80−0.91 (48H, m), 1.20−1.56 (96H, m), 1.60−1.82 (32H, m), 2.68−2.85 (32H, m), 6.69 (2H, s), 6.90−7.13 (18H, m), 7.60 (1H, s). GPC: M_w (19×10^3 g/mol), PDI (1.37).

Characterization. *Hole Mobility Measurement.* Hole mobility was measured by using a diode configuration of ITO/PEDOT:PSS/polymer/Al by taking current−voltage current in the range of 0−6 V and fitting the results to a space charge limited form; the SCLC is described by

$$J = 9\varepsilon_0\varepsilon_r\mu V^2/8L^3$$

In this equation, ε_0 is the permittivity of free space, ε_r is the dielectric constant of the polymer, μ is the hole mobility, V is the voltage drop across the device, and L is the polymer thickness. $V = V_{appl} - V - V_{bi}$, where V_{appl} is the applied voltage to the device, V_r is the voltage drop due to contact resistance and series resistance across the electrodes, and V_{bi} is the built-in voltage due to the difference in work function of the two electrodes. The resistance of the device was measured using a blank configuration ITO/PEDOT/Al and was found to be about 10−20 Ω. The V_{bi} was deduced from the best fit of the $J^{0.5}$ vs V_{appl} plot at voltages above 2.5 V and is found to be about 1.5 V. The dielectric constant ε_r is assumed to be 3 in our analysis, which is a typical value for conjugated polymers. The thickness of the polymer films was measured by AFM.

Fabrication and Characterization of Polymer Solar Cells. The ITO-coated glass substrate was cleaned stepwise in water, acetone, and isopropyl alcohol under ultrasonication for 30 min and subsequently dried by using argon gas. The substrate was further cleaned with ultraviolet ozone for 10 min. A layer of highly conducting poly(3,4-ethylenedioxythiophene)/poly(styrenesulfonate) (PEDOT−PSS) (Baytron P from H.C. Starck) was spin-cast with a thickness of ∼100 nm (4000 rpm) from aqueous solution on ITO surface. The substrate was dried for 1 h at 60 °C under vacuum and then cooled by argon steam. The chlorobenzene solution (for **PF**) or chloroform solution (for **MF**) was composed of the oligomer or polymer and PCBM in 1:1 mass ratio (10 mg/mL for sample). These solutions were then spin-casted on top of the PEDOT-PSS layer. The thickness of the polymer film was controlled to about 100 nm by varying the rotation speed of spin-coating. Subsequently, the device was pumped down in vacuum (10^{-6} Torr), and a 80 nm thick Al electrode was deposited on the top. The area of deposited Al electrode was defined as ca. 3.14 mm^2 by a shadow mask. Current−voltage measurements were recorded with a self-made source unit under ambient atmosphere. A 96000 150 W solar simulator from the Newport Co. with an AM1.5G filter was used as the light source without calibrating the mismatch of the simulated spectrum with the solar spectrum.

Femtosecond Transient Absorption Spectroscopy. Ultrafast transient absorption (TA) spectra and kinetics were carried out at Center for Nanoscale Materials at Argonne National Laboratory using a Ti:sapphire laser system from Spectra Physics and a data acquisition system from Ultrafast Systems, Inc. The laser system consisted of an oscillator, a regenerative amplifier, and an optical parametric amplifier (OPA), which was operated at a5 kHz repetition rate. Laser pulses with a duration of 35 fs at full width at half-maximum (fwhm) and pulse energy of 10 nJ at 600 nm were obtained. The transient absorption spectrometer enables simultaneous three-dimensional data collection (spectra/kinetics/ΔOD) for probe

wavelengths of 450−750 and 850−1600 nm. The excitation wavelength was 600 nm for all samples. The optical density of each sample was <0.4 at 600 nm. The instrumental response function was 120−150 fs at fwhm. A CCD detector was used to collect the data in the spectral region of 500−750 nm while a GaAs detector was used to collect the data in the spectral region of 900−1600 nm.

Grazing Incidence X-ray Scattering Measurements. Grazing-incidence small-angle X-ray scattering (GISAXS) and wide-angle X-ray scattering (GIWAXS) measurements were carried out at Beamline 8ID of the Advanced Photon Source (APS) in Argonne National Laboratory. The photon energy of the beam was 7.35 keV. Scattering intensities are expressed as a function of the scattering vector, $q = 4\pi/\lambda \sin \theta$, where θ is the half-scattering angle and $\lambda = 1.6868$ Å is the wavelength of the incident radiation. The d-spacing of a peak is $2\pi/q$.

The samples were kept under vacuum during GISAXS and GIWAXS measurements to minimize the radiation damage to the films from the X-ray beam. A two-dimensional area MAR detector was used to collect the scattering image and was situated at 194.2 and 28.09 cm from the sample for GISAXS and GIWAXS measurements, respectively. The films were illuminated at an incidence angle of about 0.2° so that the X-ray beam could penetrate the entire thickness of the film and only the surface of the glass substrate, which minimized the background scattering from the substrate.

Acknowledgment. We gratefully acknowledge the financial support of the National Science Foundation grant (DMR-703274, L.Y.) and the NSF MRSEC program at the University of Chicago. We acknowledge the support by UC/ANL collaborative seed grant (L.Y. and L.X.C.), Northwestern University setup fund, and the Division of Chemical Sciences, Office of Basic Energy Sciences, the U.S. Department of Energy, under Contract W-31-109-Eng-38 (for L.X.C.). We thank Dr. David J. Gosztola for his help in the transient absorption facility at the Center for Nanoscale Materials of Argonne National Laboratory and Drs. Michael Sprung and Byeongdu Lee of the Advanced Photon Source for their help at the beamline setup, and useful discussions in data analysis for GIWAXS and GISAXS. The facilities of the Advanced Photon Source and the Center for Nanoscale Materials are supported by Office of Basic Energy Sciences, the U.S. Department of Energy, under Contract W-31-109-Eng-38.

References and Notes

(1) (a) Yu, G.; Gao, J.; Hummelen, J. C.; Wudl, F.; Heeger, A. J. *Science* **1995**, *270*, 1789. (b) Scharber, M. C.; Wuhlbacher, D.; Koppe, M.; Denk, P.; Waldauf, C.; Heeger, A. J.; Brabec, L. *Adv. Mater.* **2006**, *18*, 789.

(2) (a) Brabec, C. J.; Sariciftci, N. S.; Hummelen, J. C. *Adv. Funct. Mater.* **2001**, *11*, 15. (b) Coakley, K. M.; McGehee, M. D. *Chem. Mater.* **2004**, *16*, 4533.

(3) Brabec, C. J. *Sol. Energy Mater. Sol. Cells* **2004**, *83*, 273–292.

(4) (a) Li, G.; Shrotriya, V.; Huang, J. S.; Yao, Y.; Moriarty, T.; Emery, K.; Yang, Y. *Nat. Mater.* **2005**, *4*, 864. (b) Ma, W. L.; Yang, C. Y.; Gong, X.; Lee, K. H.; Heeger, A. J. *Adv. Funct. Mater.* **2005**, *15*, 1617.

(5) (a) Van Duren, J. J.; Loos, J.; Morissey, F.; Leewis, C. M.; Kivits, K. P.; Vanzendoorn, L. J.; Rispens, M. T.; Hummelen, J. C.; Janssen, R. A. J. *Adv. Funct. Mater.* **2002**, *12*, 665. (b) Jahang, W. S.; Francis, A. H.; Moon, H.; Nanos, J. I.; Curtis, M. D. *Appl. Phys. Lett.* **2006**, *88*, 093504. (c) Thompson, B. C.; Frechet, J. M. J. *Angew. Chem., Int. Ed.* **2008**, *47*, 58. (d) Irwin, M. D.; Buchholz, D. B.; Hains, A. W.; Chang, R. P. H.; Marks, T. J. *Proc. Natl. Acad. Sci. U.S.A.* **2008**, *105*, 2783.

(6) Roncali, J. *Macromol. Rapid Commun.* **2007**, *28*, 1761.

(7) (a) Svensson, M.; Zhang, F.; Veenstra, S. C.; Verhees, W. J. H.; Hummelen, J. C.; Kroon, J. M.; Inganas, O.; Anderson, M. R. *Adv. Mater.* **2003**, *15*, 988. (b) Zhou, Q.; Hou, Q.; Zheng, L.; Deng, X.; Yu, G.; Cao, Y. *Appl. Phys. Lett.* **2004**, *84*, 1653. (c) Wienk, M. M.; Turbiez, M. G. R.; Struijk, M. P.; Fonrodona, M.; Janssen, R. A. J. *Appl. Phys. Lett.* **2006**, 88. (d) Zhang, F. L.; Mammo, W.; Andersson, L. M.; Admassie, S.; Andersson, M. R.; Inganas, L.; Admassie, S.; Andersson, M. R.; Ingands, O. *Adv. Mater.* **2006**, *18*, 2169. (e) Ashraf, R. S.; Shahid, M.; Klemm, E.; Al-Ibrahim, M.; Sensfuss, S. *Macromol. Rapid Commun.* **2006**, *27*, 1454. (f) Muhlbacher, D.; Scharber, M.; Morana, M.; Zhu, Z. G.; Waller, D.; Gaudiana, R.; Brabec, C. *Adv. Mater.* **2006**, *18*, 2884. (g) Blouin, N.; Michaud, A.; Leclerc, M. *Adv. Mater.* **2007**, *19*, 2295. (h) Peet, J.; Kim, J. Y.; Coates, N. E.; Ma, W. L.; Moses, D.; Heeger, A. J.; Bazan, G. C. *Nat. Mater.* **2007**, *6*, 497. (i) Wienk, M. M.; Turbiez, M.; Gilot, J.; Janssen, R. J. J. *Adv. Mater.* **2008**, *20*, 2556.

(8) (a) Wudl, F.; Kobayashi, M.; Heeger, A. J. *J. Org. Chem.* **1984**, *49*, 3382. (b) Pomerantz, M.; Chalonner-Gill, B.; Harding, M. O.; Tseng, J. J.; Pomerantz, W. J. *J. Chem. Soc., Chem. Commun.* **1992**, 1672.

(9) (a) Pomerantz, M.; Gu, X. M. *Synth. Met.* **1997**, *84*, 243. (b) Neef, C. J.; Brotherston, I. D.; Ferraris, J. P. *Chem. Mater.* **1999**, *11*, 1957. (c) Lee, K.; Sotzing, G. A. *Macromolecules* **2001**, *34*, 5746. (d) Campos, L. M.; Tontcheva, A.; Gunes, S.; Sonmez, G.; Neugebauer, H.; Sariciftci, N. S.; Wudl, F. *Chem. Mater.* **2005**, *17*, 4031.

(10) Yao, Y.; Liang, Y. Y.; Shrotriya, V.; Xiao, S. Q.; Yu, L. P.; Yang, Y. *Adv. Mater.* **2007**, *19*, 3979.

(11) Liang, Y. Y.; Xiao, S. Q.; Feng, D. Q.; Yu, L. P. *J. Phys. Chem. C* **2008**, *112*, 7866.

(12) Kim, Y.; Cook, S.; Tuladhar, S. M.; Choulis, S. A.; Nelson, J.; Durrant, J. R.; Bradley, D. D. C.; Giles, M.; Mcculloch, I.; Ha, C. S.; Ree, M. *Nat. Mater.* **2006**, *5*, 197.

(13) McCullough, R. D.; Lowe, R. D.; Jayaraman, M.; Anderson, D. L. *J. Org. Chem.* **1993**, *58*, 904.

(14) Politis, J. K.; Nemes, J. c.; Curtis, M. D. *J. Am. Chem. Soc.* **2001**, *123*, 2537.

(15) Pommerehne, J.; Vestweber, H.; Guss, W.; Mahrt, R. F.; Bassler, H.; Porsch, M.; Daub, J. *Adv. Mater.* **1995**, *7*, 551.

(16) (a) Malliaras, G. G.; Salem, J. R.; Brock, P. J.; Scott, C. *Phys. Rev. B* **1998**, *58*, 13411. (b) Goh, C.; Kline, R. J.; McGehee, M. D.; Kadnikova, E. N.; Frechet, J. M. J. *Appl. Phys. Lett.* **2005**, *86*, 122110.

(17) (a) Yang, X.; Van Duren, J. K. J.; Janssen, R. A. J.; Michels, M. A. J.; Loos, J. *Macromolecules* **2004**, *37*, 2151. (b) Swinnen, A.; Haeldermans, I.; Vanlaeke, P.; D'Haen, J.; Poortmans, J.; D'Olieslaeger, M.; Manca, J. V. *Eur. Phys. J. Appl. Phys.* **2006**, *36*, 251.

(18) (a) Stevens, M. A.; Silva, C.; Russell, D. M.; Friend, R. H. *Phys. Rev. B: Condens. Matter Mater. Phys.* **2001**, *63*, 165213/1. (b) Klimov, V. I.; McBranch, D. W.; Barashkov, N.; Ferraris, J. *Phys. Rev. B: Condens. Matter Mater. Phys.* **1998**, *58*, 7654.

(19) (a) Hwang, I.-W.; Soci, C.; Moses, D.; Zhu, Z.; Waller, D.; Gaudiana, R.; Brabec, C. J.; Heeger, A. J. *Adv. Mater.* **2007**, *19*, 2307. (b) Kraabel, B.; Klimov, V. I.; Kohlman, R.; Xu, S.; Wang, H. L.; McBranch, D. W. *Phys. Rev. B* **2000**, *61*, 8501.

(20) You, W.; Cao, S. K.; Hou, Z. J.; Yu, L. P. *Macromolecules* **2003**, *36*, 7014.

(21) Chen, L. X.; Xiao, S.; Yu, L. *J. Phys. Chem. B* **2006**, *110*, 11730.

(22) Loewe, R. S.; Ewbank, P. C.;.; Liu, J. S.; Zhai, L.; McCullough, R. D. *Macromolecules* **2001**, *34*, 4324.

(23) Hummelen, J. C.; Knight, B. W.; LePeq, F.; Wudl, F. *J. Org. Chem.* **1995**, *60*, 532.

MA8023969